Available online at www.sciencedirect.com
SCIENCE DIRECT®
Journal of Power Sources 134 (2004) 88–94
JOURNAL OF POWER SOURCES
www.elsevier.com/locate/jpowsour

Synthesis and structural changes of $Li_xFe_yO_z$ material prepared by a solid-state method

Young Tae Lee [a], C.S. Yoon [b], Yun Sung Lee [c], Yang-Kook Sun [a,*]

[a] *Department of Chemical Engineering, Center for Information and Communication Materials, Hanyang University, Seongdong-Gu, Seoul 133-791, South Korea*

[b] *Department of Materials Science and Engineering, Center for Information and Communication Materials, Hanyang University, Seoul 133-791, South Korea*

[c] *Faculty of Applied Chemical Engineering, Chonnam University, Kwangju 500-757, South Korea*

Available online 13 April 2004

Abstract

Lithium iron oxides ($Li_xFe_yO_z$) have been synthesized using LiOH and α-FeOOH by a solid-state method at various temperatures (200–800 °C). The lithium iron oxide obtained at 200 °C is composed of three types of structure namely, α-$LiFe_5O_8$, β-$LiFe_5O_8$, and a trace of cubic α-$LiFeO_2$. It exhibits not only a high initial discharge capacity 215 mAh g^{-1}, but also excellent cycling retention from the 11th to the 50th cycle (95%) between 1.5 and 4.5 V. On the other hand, the powder obtained at 800 °C has a well-developed, single α-$LiFeO_2$ phase and gives a very poor cycle performance below 5 mAh g^{-1} under the same test conditions. It is also found that lithium iron oxide obtained at 200 °C is first transformed into the spinel $LiFe_5O_8$ phase and is then converted into the tetragonal $LiFeO_2$ phase after a long-term cycling. It is suggested that the tetragonal $LiFeO_2$ phase might assist the stabilization of the original lithium iron oxide structure on cycling.

Keywords: Discharge capacity; Lithium iron oxide; Cycling performance; Structural change; Lithium battery

1. Introduction

Secondary lithium batteries have become attractive power sources for portable electronic devices, such as laptop computers and cellular phones, due to their high volumetric and gravimetric energy densities compared with those of other rechargeable battery systems. Transition metal oxides are promising candidates for positive electrodes (cathodes) for lithium secondary batteries. Many research groups have investigated various of these cathode materials such as $LiMO_2$ (M = Co, Ni, Mn, Fe, ...) [1,2].

It is well known that $LiFeO_2$ has different forms, i.e, the α-, β-, and γ- conjugated forms, as determined by the method and conditions of synthesis. The α-$LiFeO_2$ is a cubic unit cell of space group *Fm*3*m*, and β-$LiFeO_2$ (monoclinic, C2/*c*) is formed by an intermediate phase during the ordering process. The γ-$LiFeO_2$ (tetragonal, $I4_1/amd$) is obtained by reducing the symmetry from cubic to tetragonal by ordering the Li^+ and Fe^{3+} ions at octahedral sites. The conjugated $LiFeO_2$ (orthorhombic, *Pmnm*) is synthesized by the H^+/Li^+ ion-exchange reaction from γ-FeOOH at a reaction temperature of 100–500 °C [3–11].

Recently, Tabuchi et al. [9] reported a new form of metastable lithium iron oxides ($Li_{1-x}Fe_{5+x}O_8$), which was synthesized using α-$NaFeO_2$ and LiCl in ethanol by the solvothermal reaction at a low reaction temperature (220 °C). The lithium iron oxide was formed as a solid solution of Fe_3O_4 ($Fd\bar{3}m$, a = 8.396 Å) and β-$LiFe_5O_8$ ($Fd\bar{3}m$, a = 8.333 Å) by means of various analysis techniques. These workers also disclosed that the oxidation state of lithium iron oxide was reduced from 3+ during a long synthetic reaction process and that the movement of Fe^{3+} ions to tetrahedral sites in a *ccp* oxygen array disturbed the easy preparation of the lithium iron oxide material [9].

In other studies, Kim and Manthiram [12] reported that nano-crystalline lithium iron oxide ($Li_xFe_yO_z$) of an amorphous type yields a high discharge capacity of about 140 mAh g^{-1} with a fairly good cycleability in the range of 1.5–4.3 V. Various types of lithium iron oxide with Li:Fe ratio of 0.69–1.22 were synthesized by means of the solution method. The method utilized the oxidation reaction of Fe^{2+} with lithium peroxide in the presence of excess lithium

* Corresponding author. Tel.: +82-2-2290-0524; fax: +82-2-2282-7329.
E-mail address: yksun@hanyang.ac.kr (Y.-K. Sun).

0378-7753/$ – see front matter © 2004 Elsevier B.V. All rights reserved.
doi:10.1016/j.jpowsour.2004.02.001

hydroxide in an aqueous medium. Although the procedure successfully obtained lithium iron oxide with a fairly good battery performance at low temperature (200 °C), the cycle characteristics were inadequate for the material to serve as a practical cathode in lithium secondary batteries [12].

Given the above findings, the present study was initiated to develop an easy method for the synthesis of a new type of lithium iron oxide, with an excellent cycling performance, via a conventional solid-state reaction. Moreover, the existence of any structural transformations in the lithium iron oxide system, which could be a key factor in the understanding the cyclic behaviour of the $Li/Li_xFe_yO_z$ system, has been investigated.

2. Experimental

Lithium iron oxides ($Li_xFe_yO_z$) were synthesized from $LiOH{\cdot}H_2O$ (Aldrich Chemical, USA) and α-FeOOH (Aldrich Chemical, USA) under a nitrogen atmosphere by a solid-state method. Stoichiometric amounts (Li:Fe = 1.0) of the starting materials were thoroughly ground in a mortar for 1 h. The mixture was pre-calcined at 100 °C for 12 h in nitrogen, and then ground again in a mortar for 30 min. The intermediate powder was pressed into a pellet then calcined at various temperatures (200–800 °C) for 12 h in a nitrogen atmosphere. The contents of Li and Fe in the resulting material were analyzed by means of an inductively coupled plasma spectrometer (ICP, SPS7800, Seiko Instrument, Japan) by dissolving the powder in dilute nitric acid.

Powder X-ray diffraction (XRD, Rint-2000, Rigaku, Japan) using Cu Kα radiation was used to identify the crystalline phases of the synthesized materials and cycled electrodes. The particle size and morphology of the compounds were observed with a field emission scanning electron microscope (FE-SEM, S-4700, Hitachi, Japan). A transmission electron microscope (TEM, JEM2010, JOEL, Japan), equipped with energy-dispersive X-ray spectrometer (EDS), was employed to characterize the microstructure of the electrode after charge–discharge cycling.

Electrochemical characterization was conducted with CR2032 coin-type cells. The cathode was fabricated with 20 mg of active material and 12 mg of conductive binder (8 mg of Teflonized acetylene black (TAB) and 4 mg of graphite). It was pressed at 300 kg cm^{-2} on to a stainless-steel mesh (200 mm^2), which served as a current collector, and then dried at 150 °C for 5 h in an vacuum oven. The test cell comprised the cathode and a lithium metal anode (Cyprus Foote Mineral Co.) that were separated by a porous polyethylene (PE) film. The electrolyte was a mixture of 1 M $LiPF_6$–ethylene carbonate (EC)/dimethyl carbonate (DMC) (1:2 by volume, Ube Chemicals, Japan). The charge and discharge current density was 0.2 mA cm^{-2} with a cut-off voltage of 1.5–4.5 V at room temperature.

3. Results and discussion

Chemical analysis showed that the ratio of cations (Li and Fe) in the resulting powder was 1.0. The X-ray diffraction (XRD) patterns of the powders calcined at various temperatures are presented in Fig. 1. The lithium iron oxide obtained at 200 °C (Fig. 1a) has a broad reflection pattern, which indicates a polymorphous structure with poor crystallinity, small particle-size, and an amorphous-like phase. It is very difficult to distinguish the original structure due to the low crystallinity and some impurities over whole scan range. The intermediate compounds (300 and 400 °C) are gradually transformed into a mixture of $LiFe_5O_8$ spinel and α-$LiFeO_2$ phases. In addition, the XRD pattern obtained at 400 °C exhibits stronger α-$LiFeO_2$ diffraction peaks, such as (1 1 0), (2 0 0) and (2 2 0), than that of the 300 °C sample. The compound obtained at 800 °C shows a single cubic α-$LiFeO_2$ phase (Fig. 1d), and it is well known that it is difficult to insert/extract lithium into and out of this structure.

In order to investigate the original structure of the as-prepared lithium iron oxides, transmission electron microscopy analysis was performed. TEM bright-field images and an electron diffraction pattern for the lithium iron oxide obtained at 200 °C are given in Fig. 2. The bright-field images show that the powder consists of an agglomeration fine particles with a size less than 20 nm. In addition, the particle shapes are not well-defined which suggests that the powder is poorly crystallized in agreement with the XRD data. The polycrystalline ring pattern seen in Fig. 2c alone is sufficient to identify conclusively the structure of the as-prepared powder partly due to the numerous polymorphs of lithium iron oxides. Two strong peaks, however, suggest that the as-prepared material has one of following cubic

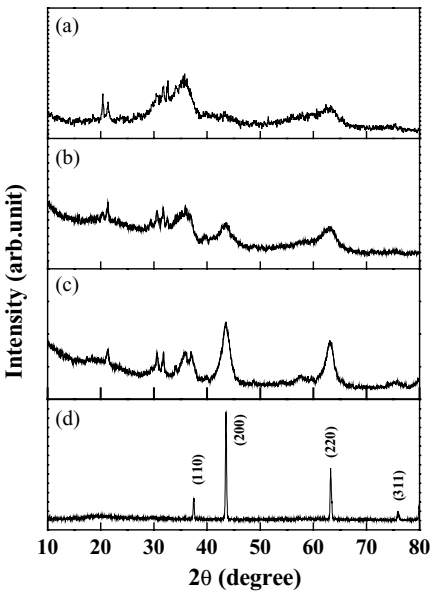

Fig. 1. X-ray diffraction patterns for $Li_xFe_yO_z$ powders obtained at (a) 200 °C, (b) 300 °C, (c) 400 °C, (d) 800 °C.

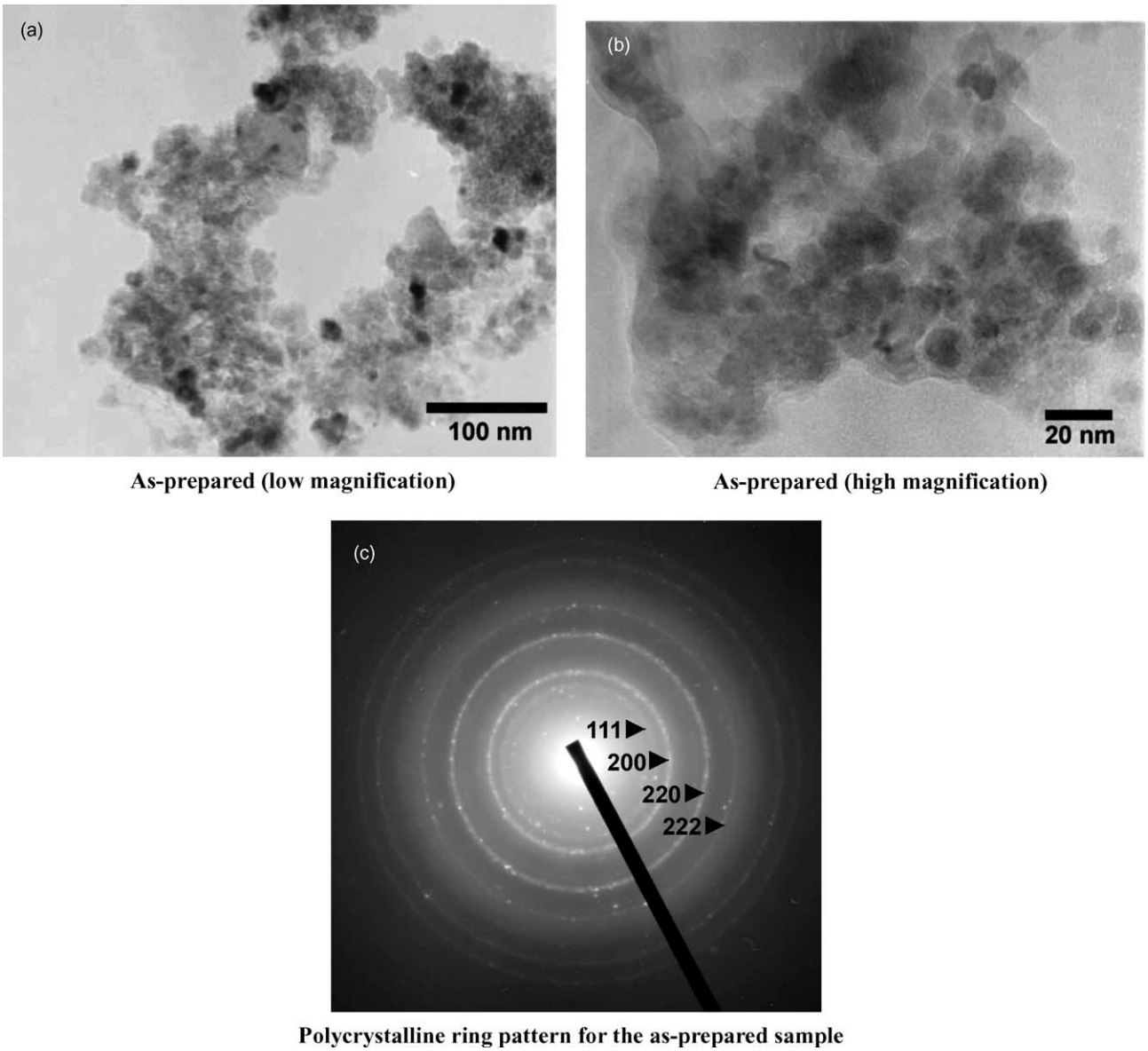

Fig. 2. (a) TEM bright-field image of lithium iron oxide powder prepared at 200 °C, (b) magnified image of (a) showing the crystal size, (c) polycrystalline electron diffraction pattern obtained from same powder.

structure [5]: α-$LiFeO_2$ (*Fm*3*m*), α-$LiFe_5O_8$ ($P4_132$, ordered high temperature phase), or β-$LiFe_5O_8$(*Fd*3*m*). The pattern in Fig. 2c has been indexed based on the α-$LiFeO_2$ structure because of the absence of the strong (3 1 1) peak. The powder could, however, well be a mixture of different cubic phases. Tabuchi et al. [9] have reported that a single $LiFe_5O_8$ compound synthesized at 220 °C is the metastable β-phase and it can be transformed into α-$LiFe_5O_8$ at 700 °C by consecutive calcinations. By contrast, the lithium iron oxide obtained at 200 °C in this study has two types of $LiFe_5O_8$ phase, which is changed from $LiFe_5O_8$ to the α-$LiFeO_2$ phase when the synthesis temperature is increased (800 °C).

The morphologies of the powder obtained at various temperatures were observed with a scanning electron microscope, see Fig. 3. The powder obtained at 200 °C has a nano-crystalline size; it is composed of small particle sizes of about 10–20 nm. On the other hand, the α-$LiFeO_2$ powder obtained at 800 °C (Fig. 3d) has greater particle size of about 700–800 nm and a slightly different particle shape. The average particle size of the powder obtained at 800 °C is 20 times that of the powder obtained at 200 °C. Because the particle size and specific surface-area are strongly related to stabilization of the cycle performance of lithium secondary batteries, it can be assumed that these two materials may present quite different electrochemical behaviour during cycle testing. Moreover, it is considered that the cathode material obtained at 200 °C with a smaller particle size in this study, especially with a nano-crystalline size, may exhibit a high discharge capacity (with higher specific surface-area)

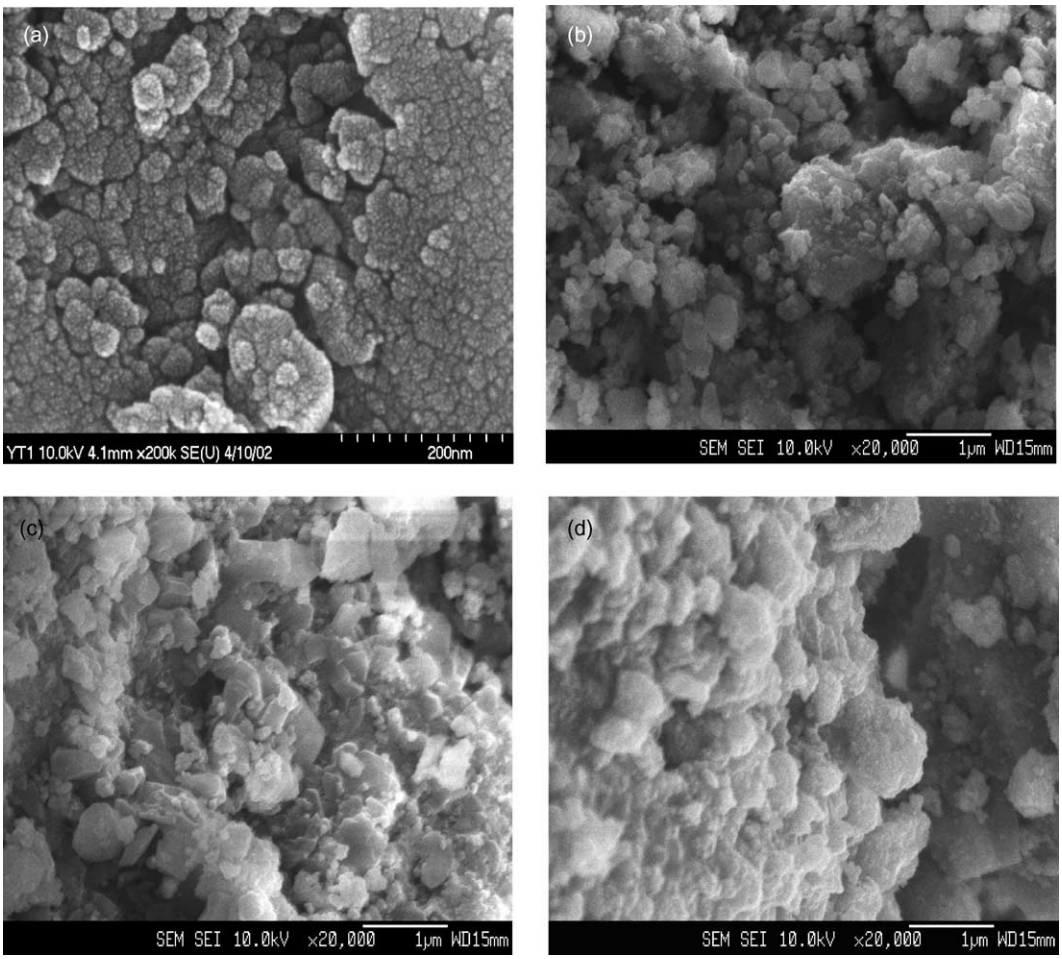

Fig. 3. Scanning electron micrographs of $Li_xFe_yO_z$ powders obtained at (a) 200 °C, (b) 300 °C, (c) 400 °C, (d) 800 °C.

and good structure stability by reducing the volume expansion during lithium insertion/extraction into/from the iron structure [12–14].

The charge–discharge curves of $Li/Li_xFe_yO_z$ cells obtained at various calcination temperatures are given in Fig. 4. The first charge curve for the cell with $Li_xFe_yO_z$ obtained at 200 °C rapidly increases up to 4.0 V (Fig. 4a) This cell shows a small plateau region at about 4.1 V and exhibits another long voltage plateau between 4.2 and 4.3 V. While the first discharge curve falls drastically to 3.3 V, it shows two small voltage plateaus between 2.0 and 1.5 V. For the second cycle, the voltage profile gradually decreases without any remarkable voltage plateaux and exhibits a slightly different shape compared with of the first cycle. The $Li/Li_xFe_yO_z$ cell obtained at 300 °C (Fig. 4b) displays very similar cycling behaviour to that of the sample obtained at 200 °C.

On the other hand, the $Li/Li_xFe_yO_z$ obtained at 400 °C (Fig. 4c) displays a different electrochemical characteristics compared with those of the lithium iron oxide materials obtained at lower temperatures (200 and 300 °C). First, there are no voltage plateaux in the first discharge curve. Second, the cell gives a very small discharge capacity. Finally, the discharge capacity increases upon cycling, although the amount of the increase is very small. These differences suggest that lithium iron oxide obtained at 400 °C has very different characteristics to those of material obtained at lower temperatures. It is considered that the main reason for these unique characteristics is the growth of the $LiFeO_2$ (β- or γ-form) phase at 400 °C [15].

The lithium iron oxide material obtained at 800 °C shows a very small discharge capacity of 5 mAh g^{-1} after 50 cycles. This poor performance strongly supports the phase transformation of β- or γ-$LiFeO_2$ into inactive α-$LiFeO_2$ material at high temperature (800 °C). This conclusion is confirmed by the XRD results shown in Fig. 1. Therefore, it is considered that the amount of electrochemically active spinel-like phases, such as (α- or β-) $LiFe_5O_8$ in the structure, gradually decreases as the calcination temperature increases, which induces an abrupt decrease in the initial discharge capacity of the lithium iron oxide system.

The variation in the specific discharge capacity with the number of cycles for the lithium iron oxide materials obtained at various temperatures is shown in Fig. 5. The charge–discharge current density is 0.2 mA cm^{-2} with a cut-off voltage of 1.5–4.5 V at room temperature. The lithium iron oxide material obtained at 200 °C gives the

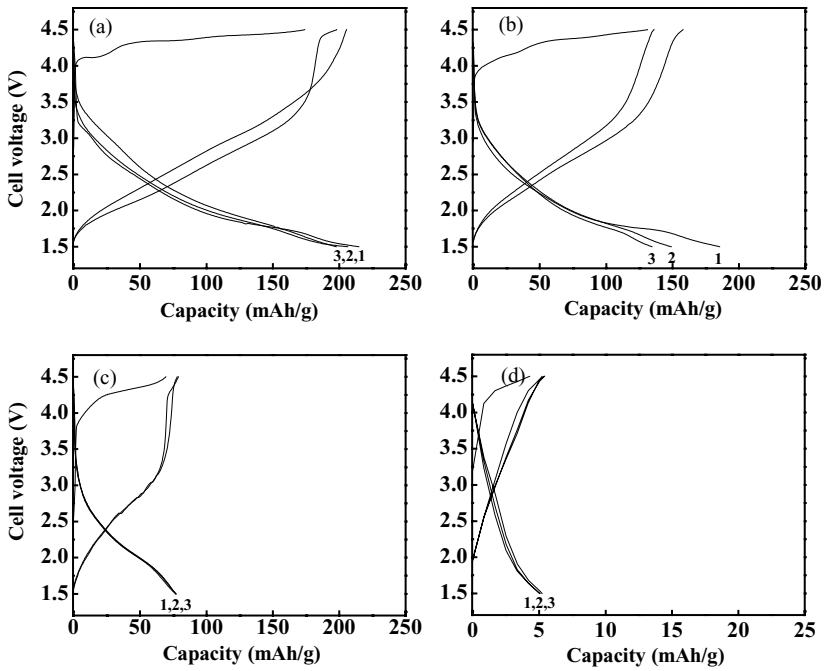

Fig. 4. Charge–discharge curves of $Li_xFe_yO_z$ powders prepared at (a) 200 °C, (b) 300 °C, (c) 400 °C, (d) 800 °C. Test conditions were a current density of 0.2 mA cm^{-2} between 1.5 and 4.5 V at 25 °C.

highest initial discharge capacity of 215 mAh g^{-1} as well as an excellent cycle retention rate from the 11th to the 50th cycle is 95%, which is the highest value that has been previously reported.

The data in Fig. 5 appears to show same unique characteristics. The lithium iron oxide materials obtained at low temperature (200 and 300 °C) showed a large capacity drop during the early stages and then maintains an excellent cycling performance for 50 cycles. By contrast, the other two lithium iron oxide materials have a large amount of inactive

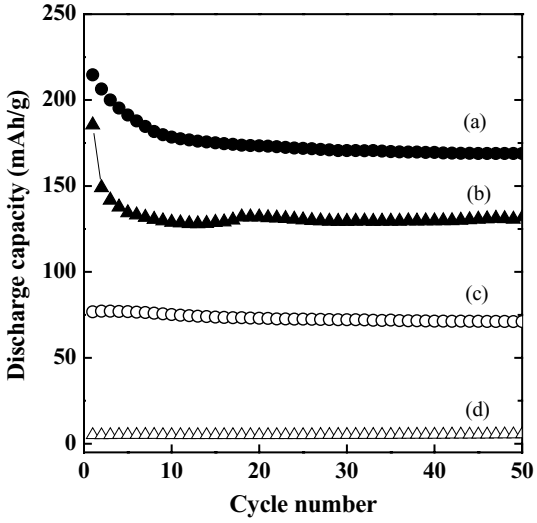

Fig. 5. Specific discharge capacity vs. number of cycles for $Li/Li_xFe_yO_z$ cells obtained at (a) 200 °C, (b) 300 °C, (c) 400 °C, (d) 800 °C.

α-$LiFeO_2$ (400 °C) or single α-$LiFeO_2$ (800 °C) phase and exhibit no abrupt capacity loss during the entire cycling test. This suggests that the powders obtained at lower temperatures might have produced a structural change in the early stages of cycling which gives a high possibility to induce different cycle characteristics.

In order to investigate this unique cycle behaviour of the two types of lithium iron oxides, ex situ XRD measurements were taken on four electrodes obtained at 200 °C in the discharged state after various cycles, i.e., on electrodes that display the most severe capacity drop in the early stages (Fig. 5). The samples are kept in a glove-box for 2 days to reach equilibrium after being tested from 1.5 to 4.5 V. The XRD patterns are shown in Fig. 6, and are examined in two groups to explain easily the relation between the structural change and cycling behaviour. One group (1st and 3rd cycles) present almost the same XRD patterns, which are representative of a mixture of $LiFe_5O_8$ and a small amount of the $LiFeO_2$ phase. Although it is difficult to distinguish clearly the type of $LiFeO_2$ phase between the α- and β-phases due to the low crystallinity and some impurities, the main XRD peaks for two types of $LiFeO_2$ can be distinguished, such as the (2 0 0) and (2 2 0) peaks for α- and β-$LiFeO_2$ (α-: JCPDS# 17-938, β-: JCPDS# 17-936) at $2\theta = 43.3^\circ$. The other group (15th and 50th cycles) also exhibits similar XRD patterns over the whole scan range. Two electrodes show the typical (3 1 1) and (4 4 0) peaks of the $LiFe_5O_8$ phase with an additional tetragonal (β- or γ-) $LiFeO_2$ phase ($I4_1/amd$, $Z = 4$, $a = 4.152$ Å, $c = 4.192$ Å, or $a = 4.057$ Å, $c = 8.759$ Å). The intensity of the tetragonal $LiFeO_2$ phase increases as the cycling proceeds. Based on these results, it

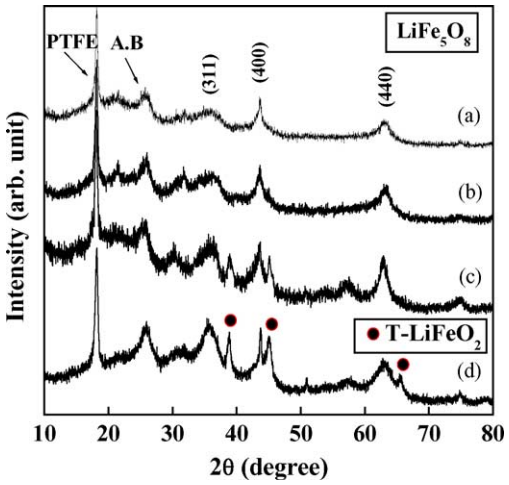

Fig. 6. Ex situ XRD patterns for cycled $Li_xFe_yO_z$ electrodes obtained at 200 °C: (a) 1st cycle, (b) 3rd cycle, (c) 15th cycle, (d) 50th cycle.

is concluded that the fairly large capacity fading during the early stages of the cell using $LiFeO_2$ prepared at 200 °C is due to the spinel transformation. On the other hand, the $Li/Li_xFe_yO_z$ cell after the 10th cycle exhibits a very stable cycle characteristic, due to the appearance of the tetragonal $LiFeO_2$ phase. A similar structure change on cycling has been reported for the orthorhombic $Li|LiFeO_2$ system. Lee et al. [16] found that the orthorhombic $Li|LiFeO_2$ system undergoes an almost complete conversion to the $LiFe_5O_8$ spinel phase after 50 cycles. Based on this investigation, they suggested that the structural change from orthorhombic to spinel is the main cause of the capacity decline of the $Li|LiFeO_2$ system. Similarly, the $Li/Li_xFe_yO_z$ cell examined in this study also reveals a severe capacity loss during spinel transformation in the early stages. One unique characteristic of the $Li/Li_xFe_yO_z$ cell in this study is that a new structural change occurs from the spinel to tetragonal phase after the structural change to the spinel $LiFe_5O_8$ in the early stages. The structural change continues even after long-term cycling and results in a mixed phase of spinel $LiFe_5O_8$ and tetragonal $LiFeO_2$ after the 50th cycle.

In order to reveal this structural change in a different way, TEM analysis was conducted on the same electrodes that were examined by ex situ XRD. Unfortunately, it was not possible to obtain a reasonable result that could clearly show the structural changes from the 1st to the 50th cycle. This is because, after the 50th cycle, the particles are seriously broken due to lithium insertion/extraction during long-term cycling. The particle size of the electrode after 50 cycles is shown in Fig. 7. It can be seen that the particles have become even smaller after cycling. From TEM analysis, it confirmed that the main structure of the electrode after 50 cycles is very similar to that of the tetragonal β-$LiFeO_2$ phase. At present, there is no concrete explanation as to why nano-crystalline lithium iron oxide partially transforms into the tetragonal $LiFeO_2$ phase and what is the role of the tetragonal phase to improve the cycling performance of the $Li/Li_xFe_yO_z$ system. Further work involving the transformation mechanism is now in progress.

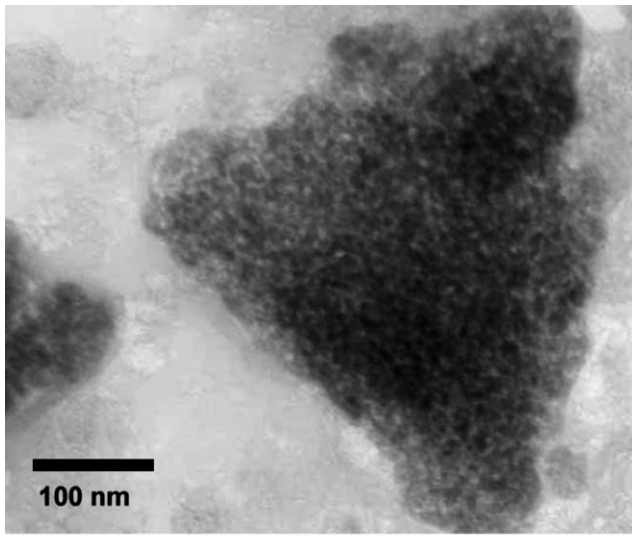

After cycle

Fig. 7. TEM bright-field image of cycled electrode.

4. Conclusions

Lithium iron oxides, $Li_xFe_yO_z$, have been synthesized using $LiOH{\cdot}H_2O$ and α-FeOOH at various temperatures (200–800 °C) by a solid-state reaction method. Nano-crystalline lithium iron oxide obtained at 200 °C gives a high initial discharge capacity (215 mAh g^{-1}) and a fairly good capacity retention rate at room temperature, although it exhibited a gradual fall in until the 10th cycle. It is found that the decrease in the initial capacity of the $Li/Li_xFe_yO_z$ cell examined in this study is due to the growth of inactive α-$LiFeO_2$ material. Furthermore, it is revealed that lithium iron oxide obtained at 200 °C partially transforms into the tetragonal $LiFeO_2$ phase after formation of the spinel $LiFe_5O_8$ in the early stages. It is suggested that this second transformation contributes to the stabilization of the host structure.

Acknowledgements

This work has been supported by EESRI (03-27), which is funded by MOCIE (Ministry of Commerce, Industry and Energy).

References

[1] K. Mizushima, P.C. Jones, P.J. Wiseman, J.B. Goodenouh, Mater. Res. Bull. 15 (1980) 783.
[2] T. Nagaura, K. Tazawa, Prog. Batt. Sol. Cells 9 (1990) 20.

[3] R. Kanno, T. Shirane, Y. Kawamoto, Y. Takeda, M. Takano, M. Ohashi, Y. Yamaguchi, J. Electrochem. Soc. 146 (1996) 2435.
[4] T. Shirane, R. Kanno, Y. Kawamoto, Y. Takeda, M. Takano, T. Kamiyama, F. Izumi, Solid State Ionics 79 (1995) 227.
[5] M. Tabuchi, K. Ado, H. Sakaebe, C. Masquelier, H. Kageyama, O. Nakamura, Solid State Ionics 79 (1995) 220.
[6] M. Tabuchi, C. Masquelier, T. Takeuchi, K. Ado, I. Matsubara, T. Shirane, R. Kanno, S. Tsutsui, S. Nasu, H. Sakaebe, O. Nakamura, Solid State Ionics 90 (1996) 129.
[7] K. Ado, M. Tabuchi, H. Kobayashi, H. Kageyama, O. Nakamura, Y. Inaba, R. Kanno, M. Takagi, Y. Takeda, J. Electrochem. Soc. 144 (1997) L177.
[8] M. Tabuchi, S. Tsutsui, C. Masquelier, R. Kanno, K. Ado, I. Matsubara, S. Nasu, H. Kageyama, J. Solid State Chem. 140 (1998) 159.
[9] M. Tabuchi, K. Ado, H. Kobayashi, I. Matsubara, H. Kageyama, M. Wakita, S. Tsutsui, S. Nasu, Y. Takeda, C. Masqulier, A. Hirano, R. Kanno, J. Solid State Chem. 141 (1998) 554.
[10] Y. Sakurai, H. Arai, S. Okada, J. Yamaki, J. Power Sources 68 (1997) 711.
[11] Y. Sakurai, H. Arai, J. Yamaki, Solid State Ionics 29 (1998) 113–115.
[12] J. Kim, A. Manthiram, J. Electrochem. Soc. 146 (1997) 4374.
[13] A. Manthiram, C. Tsang, J. Electrochem. Soc. 143 (1996) L143.
[14] C. Tsang, A. Manthiram, J. Electrochem. Soc. 144 (1997) 520.
[15] J.C. Anderson, M. Schieber, J. Phys. Chem. Solids 25 (1964) 961.
[16] Y.S. Lee, C.S. Yoon, Y.K. Sun, K. Kobayakawa, Y. Sato, Electrochem. Commun. 4 (2002) 727.